MATERIALS RESEARCH LETTERS

Mater. Res. Lett., 2015
Vol. 3, No. 3, 121–127, http://dx.doi.org/10.1080/21663831.2014.999953

Taylor & Francis
Taylor & Francis Group

www.tandfonline.com/toc/tmrl20/current

Flow Stress in Submicron BCC Iron Single Crystals: Sample-size-dependent Strain-rate Sensitivity and Rate-dependent Size Strengthening

Rui Huang[a], Qing-Jie Li[b], Zhang-Jie Wang[a], Ling Huang[a], Ju Li[a,c,d], Evan Ma[a,b] and Zhi-Wei Shan[a]*

[a]*Center for Advancing Materials Performance from the Nanoscale (CAMP-Nano) & Hysitron Applied Research Center in China (HARCC), State Key Laboratory for Mechanical Behavior of Materials, Xi'an Jiaotong University, Xi'an 710049, People's Republic of China;* [b]*Department of Materials Science and Engineering, Johns Hopkins University, Baltimore, MD 21218, USA;* [c]*Department of Nuclear Science and Engineering, Massachusetts Institute of Technology, 77 Massachusetts Avenue, Cambridge, MA 02139, USA;* [d]*Department of Materials Science and Engineering, Massachusetts Institute of Technology, 77 Massachusetts Avenue, Cambridge, MA 02139, USA*

(*Received 17 September 2014; final form 12 December 2014*)

Through *in situ* scanning electron microscope microcompression tests, we demonstrated that the strain-rate sensitivity of body-centered cubic single crystal iron pillars will be reduced by one order when the pillar size was reduced from 1000 to about 200 nm. In addition, size-strengthening exponent exhibited obvious strain-rate dependence. We propose that the observed behavior is a result of the high stresses required to induce curvature bowout of dislocation arms at small sample or grain sizes, which overwhelms the lattice friction stress contribution and diminishes the role played by the mobility difference between edge and screw dislocations.

Keywords: single-crystal α-Fe, size effect, strain-rate sensitivity, Orowan equation, source truncation hardening

The flow stress of BCC metals is well known to be dependent on the strain rate imposed. The activated process underlying this strain-rate sensitivity (m) can be understood as follows [1–10]: unlike FCC metals in which both screw and edge dislocations have a planar core structure, the screw dislocations in BCC metals have a multi-plane core structure. The resulting difficulty in their slip makes the movement of screw dislocations much slower than edge dislocations and hence the rate-limiting process under normal plastic deformation conditions. However, the strain-rate sensitivity of BCC metals was found to decrease with the reduction in grain size, especially in the ultrafine-grained and nanocrystalline regimes.[1,11–13] To understand this trend, Wei et al. [11,12] used the $m \sim 1/\sqrt{\tau}$ scaling relation to explain the grain size effect on m based on the Hall–Petch-type elevation of the flow stress (τ) at small grain sizes. More recently, Cheng et al. [2] proposed an alternative explanation. They characterized the type (screw, edge or mixed) and density of the residual dislocations in nanocrystalline Mo prepared through high-pressure torsion: mixed and edge dislocations were observed to be the predominant types for grains with sizes below $\sim$100 nm. Based on their observation, Cheng et al. [2] proposed that in such grains the motion of edge and mixed dislocations becomes the rate-controlling defect process in plastic deformation, in lieu of screw dislocations. The plasticity processes mediated by edge/mixed dislocation types are believed to have low rate sensitivity such that the effective m observed in nano-grained BCC metals is small. However, we noted that even in the grain size regime where screw dislocations remain populous, m is already much lower than that in large-grained BCC metals.[2,11] In addition, almost all previous studies of the size dependence of m of BCC metals used polycrystalline materials except the one by Schneider et al.[14] They found that submicron-sized single crystal Mo pillars exhibited strain-rate sensitivity similar to their bulk counterpart. Moreover, compared with the widely studied size-strengthening effect and its underlying mechanism of single crystal BCC metals,[5,6,14–21] much less work have been carried out on m. Recently,

*Corresponding author. Emails: zwshan@mail.xjtu.edu.cn, liju@mit.edu, ema@jhu.edu

we demonstrated through molecular dynamics simulation [19] that very high applied stresses can diminish the velocity difference between screw and edge dislocations in single crystal Mo. As a consequence, BCC Mo behaves more like an FCC metal. This was supported by the fact that when their diameters were reduced below 200 nm or so, single crystal Mo pillars exhibited a higher size-strengthening exponent and mechanical annealing.[19] This prompted us to surmise that the similarities between FCC and BCC metals under high stresses may also manifest in terms of a reduced m, that is, it is the high deformation stress at small sample or grain sizes instead of other factors that cause the reduced m for nanostructured BCC metals, including single crystal BCC metals.

In addition, it has been proposed previously that the sample-size-strengthening exponent α of BCC metals increases with a decrease in the 'critical temperature',[17] defined as the temperature above which the strain rate has little effect on the flow stress of BCC metals because screw and edge dislocations have equal mobility. However, as shown in Table 1, the α for single crystal Mo ranges from 0.29 to 1.0 [5,6,16,18,19] and that for single crystal Nb is from 0.48 to 1.07.[5,6,16] Apparently, just the critical temperature argument cannot rationalize the large scatter of α observed in different BCC metals (Table 1), neither can it explain the size effect on m.

In this work, we choose BCC Fe single crystals as our model material. The sample was acquired from German Tech Co., Ltd. The dimensions of the as-received iron are 3 mm × 2.5 mm × 0.1 mm. A series of [001]-oriented α-Fe pillars with their free-end diameter D ranging from about 200 to 1030 nm and their length-to-diameter ratio of about 3:1 were fabricated using focused ion-beam (FIB) micromachining. More details about the sample preparation procedure are described in [19,22,23]. *In situ* compression tests were carried out in the chamber of the same FIB under SEM mode using a Hysitron PI85 PicoIndenter equipped with flat diamond punches, 1 μm in diameter for pillars with sizes smaller than 500 nm and 7 μm in diameter for pillars larger than 500 nm. All tests were performed at room temperature under displacement rate control. The data acquisition rate for the lowest strain rate has been set to be 100 per second but was adjusted to be higher for a higher strain rate to make sure that enough data points were captured. In order to investigate the residual dislocation structure, we used OmniProbe to lift out deformed samples and then thinned them down gradually with FIB to about 100 nm from both sides. After this, a Model 1040 NanoMill (Fischone Inc.) was employed to minimize the FIB-affected layer with an operation voltage of 800 V, with which the surface damage layer thickness can be reduced down to ~2 nm. The final observation was conducted inside a JEOL 2100F TEM under STEM mode which are known to be insensitive to strain contours and able to image dislocations clearly.

Four groups of samples with their nominal diameter of D = 200, 300, 475 and 1000 nm were tested under four different strain rates, ranging from $\dot{\varepsilon} = 10^{-1}$ to 10^{-4} s^{-1}. Regardless of the sample size and the strain rate used, multiple slip bands with obvious shear offsets are always observed after the uniaxial compression test. One typical example is shown in Figure 1. The slip traces which are ~45° inclined to the axial [001] direction suggest a {110}⟨111⟩-type slip system with a Schmid factor of 0.408. The initial free-end diameter of this pillar is about 462 nm (Figure 1(a)). After the compression test, a few large shear offsets can be seen clearly in the postmortem SEM image (Figure 1(b)).

Consistent with the morphology of the deformed pillars, all the engineering stress–strain curves exhibited multiple large load drops (Figure 2(a) and 2(b)), typical of displacement-controlled compression in single crystal metal pillars.[19,24] For D = 1000 nm samples, the average flow stress σ increased from about 450 MPa to about 700 MPa when the strain rate $\dot{\varepsilon}$ increased from 3.1×10^{-4} to 2.1×10^{-1} s^{-1} (Figure 2(a)). However, along with the reducing sample size, the strain-rate hardening effect decreases gradually and eventually becomes very small for 200 nm samples (Figure 2(b)). Note that

Table 1. Critical temperature (T_c) of BCC metals; data from Refs. [5,6,16,19,20,25].

Material	W	Mo	Ta	V	Nb	**α-Fe**
T_c (K)	800	480	450	380	350	**340**
T_{test}/T_c	0.37	0.62	0.66	0.78	0.85	**0.88**
Exponent α size range (nm)	0.21 [16]	0.38 [16]	0.41 [16]	0.79 [20]	0.48 [20]	**0.62–0.80**
	5000–200	*5000–350*	*3000–340*	*2000–200*	*5000–200*	***1000–200***
	0.44 [5]	0.44 [5]	0.43 [5]		0.93 [5]	***Our work***
	850–250	*800–200*	*850–400*		*900–250*	
		0.29 [19]			1.07 [6]	
		1200–200			*900–250*	
		1.00 [19]				
		200–80				

Note: T_{test} = 298 K in our experiment.

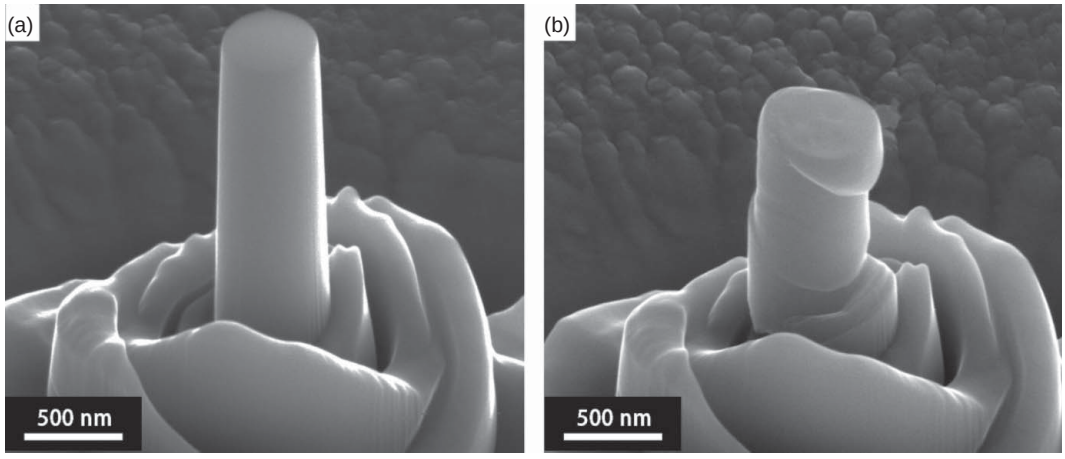

Figure 1. Representative SEM images of [001]-oriented Fe pillar before (a) and after compression (b). The initial free-end diameter is ∼462 nm.

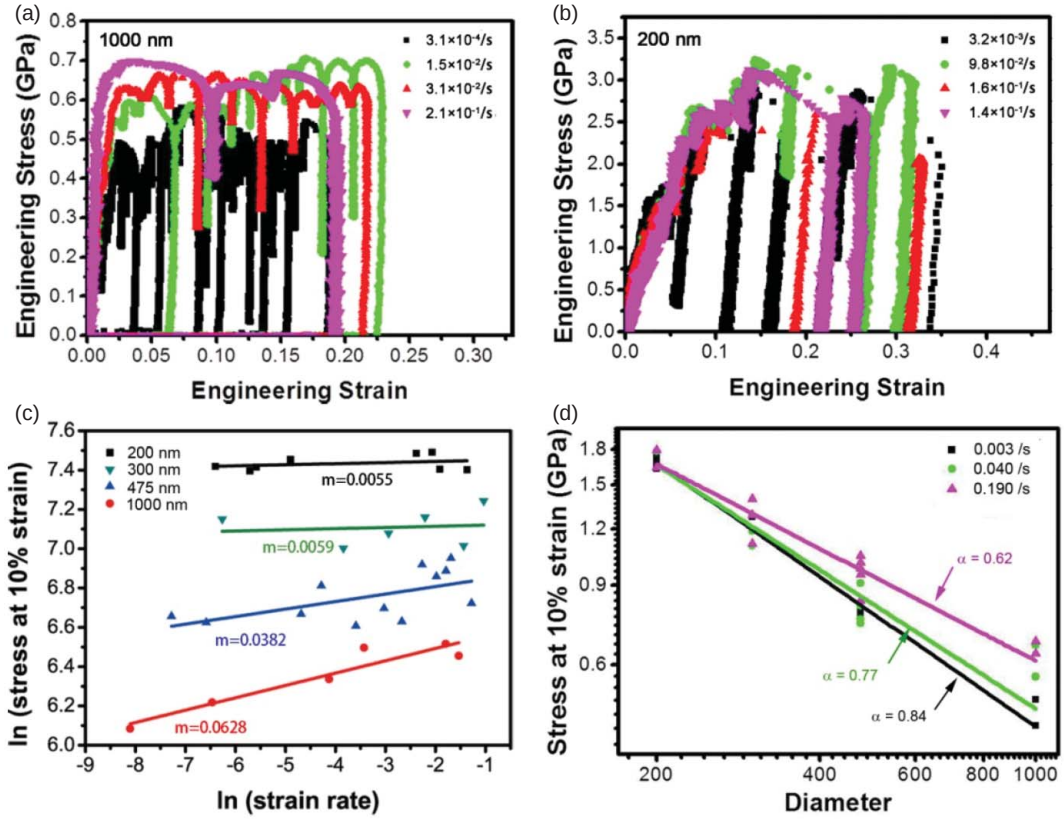

Figure 2. Size dependence of the strain-rate sensitivity of iron pillars with strain rate ranging from 10^{-4} to 10^{-1} s^{-1}. (a) and (b) are representative stress–strain curves of 1000 and 200 nm pillars, respectively. (c) Double logarithmic plot of stress at 10% strain vs. strain rate to determine *m* for single crystal Fe specimens with their diameters ranging from 200 to 1000 nm. (d) Stress at 10% strain as a function of pillar diameter for [001] oriented Fe pillars. The plot is scaled logarithmically, and shows the strain-rate dependence (three data sets for three strain rates) of the size-strengthening exponent (see linear fit of the data and corresponding exponents in the legend).

200 nm is still much larger than the dislocation-type transition size reported by Cheng et al.[2] In addition, it was interesting to note that regardless of the sample size, the frequency and the amplitude of the load drops (correspond to slip band formation, see Movie S1) decrease with increasing strain rate. The fact that the peak flow stress of $D = 1000$ nm samples ($\sim$700 MPa, Figure 2(a)) is much lower than that for $D = 200$ nm samples ($\sim$3000 MPa, Figure 2(b)) is consistent with the well-known tenet of 'smaller is stronger': $\sigma = \sigma_0 + kD^{-\alpha}$, where α is a positive exponent. The critical temperature of α-Fe is 340 K.[25] Compared

with other BCC metals, for example, W,[16] Mo,[16] Ta,[16] V [20] and Nb,[16] the critical temperature of iron is closer to room temperature (for more details, see Table 1). Therefore, it is not surprising to see that the α of iron is almost the largest among the aforementioned BCC metals (see Table 1).

In order to quantify the strain-rate effect, we chose the flow stress at 10% strain as the reference for each sample. The log–log relationship between the strain rate and the flow stress at 10% strain is plotted in Figure 2(c). Despite the scatter of the data, a trend that strain-rate sensitivity decreases with decreasing sample size can be seen clearly from the linear fit for each sample size. The strain-rate sensitivity $m \equiv \partial \ln \sigma / \partial \ln \dot{\varepsilon}$, obtained from the slope of each linear fit in Figure 2(c), decreased more than 10 times, from 0.063 to about 0.0055 when the sample size was reduced from 1000 to 200 nm. The former, that is, $m = 0.063$, is similar to that observed in bulk α-Fe.[26] Therefore, the sample size effect on m starts when the sample dimension was reduced to $\sim$1000 nm. This trend remains the same if we choose the stresses at 5% strain. We conclude that BCC iron exhibits a strong 'size' effect on m, and this 'size' D can be either the size of grains in a polycrystalline material, or the size of the specimen for a single crystal.

In addition to 'smaller is stronger' (compare Figure 2(a) and 2(b), for example), we observe that larger samples exhibited a stronger rate dependence (Figure 2(a)) and smaller samples exhibited a much weaker rate dependence (Figure 2(b)). As such, the size-strengthening exponent α measured should be a function of strain rate, rather than remaining constant. Specifically, a lower α is expected at a higher strain rate, and at a fixed lower strain rate the effective α would appear to be higher. This was confirmed by the data plotted in Figure 2(d): when $\dot{\varepsilon}$ increased from 0.003 to 0.19/s, α decreased from 0.84 to 0.62. This change in α due to strain-rate variations at least partly explain the large scatter of α observed in different BCC metals (Table 1) and should be taken into account in the analysis of size-strengthening behavior of materials, but has been rarely paid attention to before.

Because of the strong magnetism of iron, we were not able to carry out the compression tests inside TEM under proper imaging conditions. However, we have managed to check the residual dislocation structure of the deformed iron pillars, as shown in Figure 3. It was found that the residual dislocation structure in the 1000 nm samples is quite different from that of 200 nm samples. For 1000 nm pillar (Figure 3(a)), a high density of dislocations was found in a heavily deformed zone, whereas only a few dislocations are present in other areas. Figure 3(b) is the magnified STEM image of the area framed in Figure 3(a). For 200 nm pillar, however, only one residual dislocation can be found in the heavily deformed zone, as indicated by the black arrows (Figure 3(d)). This agrees well with the expected dislocation escape due to the mechanical annealing phenomena. Because of the single tilt limitation of the TEM holder used, we were not able to identify the type of this dislocation. However, its long and straight feature is the typical characteristics of screw dislocation. In addition, Zhang et al. [27] has carried out *in situ* TEM compression of single crystal Fe–3%Si pillar. They concluded that during the compression of a pillar with its initial diameter of about 120 nm, screw dislocation dominated the deformation process at high stress level. This finding suggests that for the size range we have tested, screw dislocations may still behave quite differently from edge dislocations during deformation. This is also consistent with the observation by Cheng et al. [2] that edge and mixed dislocations take over only at much smaller grain sizes ($\sim$80 nm). As such, the reduction in m may not be attributed solely to the change in the type of dominant dislocations.

In the following, we attempt to rationalize the observed size effect on m by considering two contributions to the flow stress. Generally in elemental metals when propagation of existing dislocations controls the flow behavior (nucleation is not limiting), the flow stress has two contributors:

$$\sigma(\dot{\varepsilon}) = \sigma_{\text{friction}}(\dot{\varepsilon}) + \sigma_{\text{bowout}}(\dot{\varepsilon}, L), \qquad (1)$$

where σ_{friction} is due to intrinsic lattice friction force on a moving dislocation core. In contrast, σ_{bowout} is due to dislocation–obstacle interactions, where the obstacles may be other dislocations (forest dislocation hardening), free surfaces (source truncation hardening [28]), etc. that impede dislocation line length growth. The magnitude of σ_{bowout} depends on a characteristic distance L between pinning points, which defines a critical curvature through which the dislocations have to squeeze by to propagate. σ_{friction} depends sensitively on $\dot{\varepsilon}$ ($\propto$ dislocation velocity) and temperature because of the small activation volumes of double-kink nucleation and kink migration of the dislocation core. σ_{bowout}, as exemplified by the Orowan equation $\sigma_{\text{bowout}} \propto \mu b/L$, is on the other hand microstructural length scale sensitive but less sensitive to $\dot{\varepsilon}$, because of its usually much larger activation volume involved in bowing out through a critical curvature.[29] According to the source truncation hardening [28] interpretation of 'smaller is stronger' $\sigma = \sigma_0 + kD^{-\alpha}$, $L \propto D^{\alpha}$, and L is the mobile free-arm length [28] between an internal pinning point and the surface. From Equation (1), then, we can deduce that when L is large, for example when a large single crystal of BCC metal is undergoing stage-1 easy glide, $\sigma_{\text{friction}} \gg \sigma_{\text{bowout}}$ dominates the flow stress, so $\sigma \approx \sigma_{\text{friction}}$. Then, the difficulty is in pushing the long screw segments through the crystal, not in bowing out through the sparse microstructural obstacles. In this regime, one expects a larger $m \sim 0.06$ because of

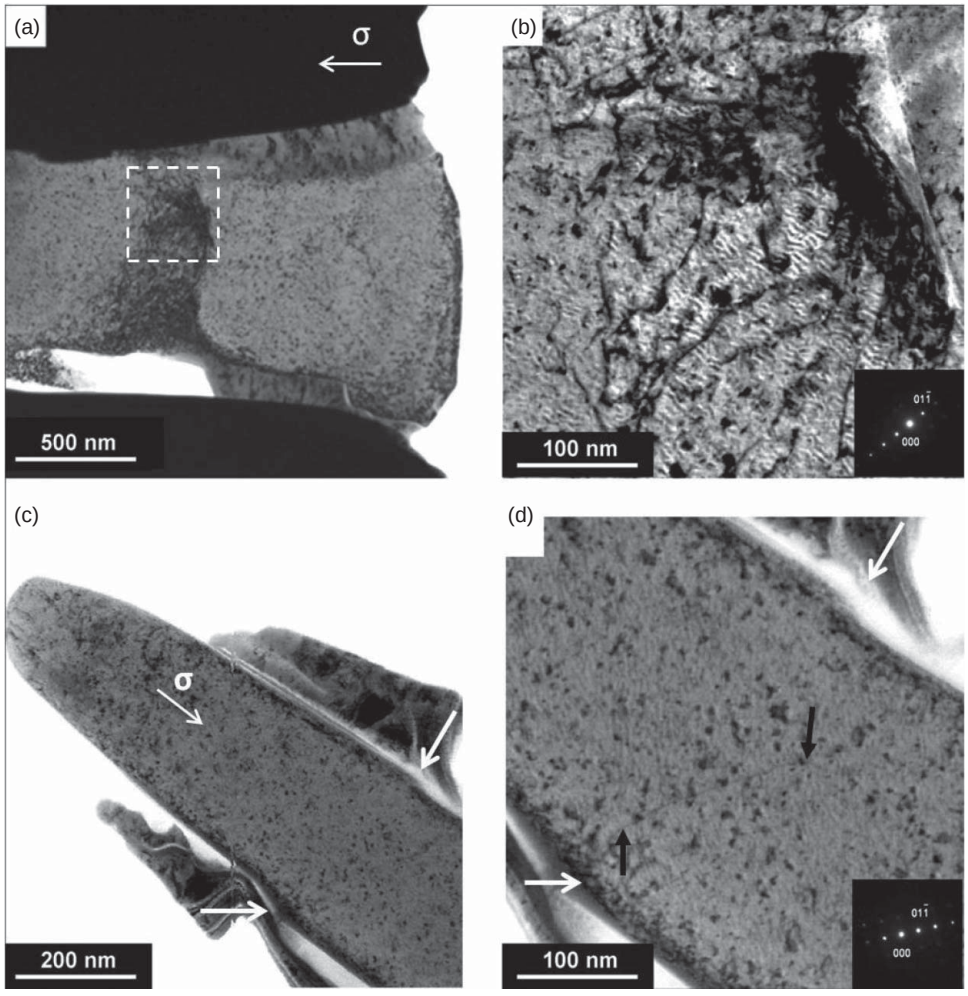

Figure 3. Typical postmortem bright-field STEM micrographs of the pillars after compression tests. (a) 1000 nm; (b) magnified image of the area framed in (a); (c) 200 nm; (d) magnified image of the area indicated by the two long white arrows in (c). Note the dislocation line marked by the two black arrows.

the intrinsically small activation volume of σ_{friction} from atomic-scale double kink nucleation and kink migration activation events. On the other hand, as L is being reduced, for example due to microstructural refinement, sample size reduction, etc., σ_{bowout} starts to overwhelm the intrinsic lattice friction, and $\sigma \approx \sigma_{\text{bowout}} \gg \sigma_{\text{friction}}$. In this regime, the difficulty lies in overcoming the critical curvature for dislocation bowout, not in whether and how the dislocation can move after the bowout. Due to the usually larger activation volume of σ_{bowout}, m will sustain a precipitous drop from ~ 0.06 to ~ 0.005 at this regime transition from friction-to-bowout controlled, as illustrated in Figure 4. In this higher stress, bowout-controlled regime, the physics that controls σ is not that different from that of FCC pillars, as the bowout formula is not very sensitive to screw or edge form. The distinction in mobility may still exist between screw and edge, but they no longer control σ.

Interestingly, after the friction-to-bowout-controlled transition, as L is further reduced, we expect m to gradually rise again, as the activation volume scales with L to some positive power.[29] In the limit of very small L (a few to tens of nanometers) and σ being a significant fraction of the ideal strength, we expect m can rise up to 0.02–0.05, which is the level expected for surface nucleation [30] (instead of propagation)-controlled flow regime. In nanocrystalline materials, $m \sim 0.02$–0.05 level is expected for slip transmission [31]-controlled mechanism across grain boundaries with large misorientation angle. When D further shrinks, one may trigger surface diffusion induced Coble creep, with m as large as 1,[32,33] as illustrated by Figure 4.

In summary, we have systematically investigated the plastic flow of [001] oriented α-Fe single crystal pillars. Their strength follows the well-established trend of 'smaller is stronger', and the size-strengthening exponent is a function of the strain rate. At the same time, the strain-rate sensitivity decreases by more than 10 times, when the sample diameter decreased from 1000 to 200 nm. Postmortem TEM observation found a high density

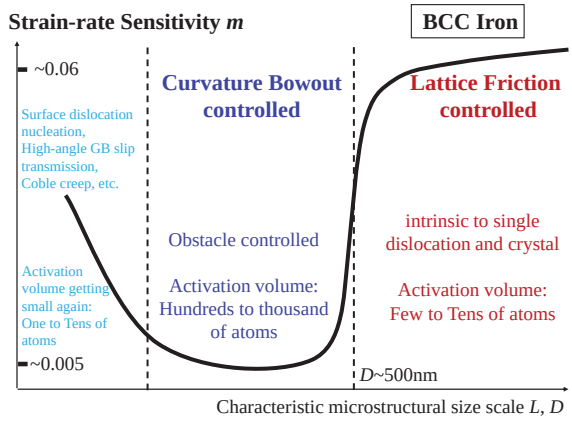

Figure 4. Regimes for strain-rate sensitivity based on characteristic microstructural size scales D. Lattice friction-controlled regime ($D > \sim 500$ nm): lattice friction of screw dislocation sensitively depends on the strain rate because of small activation volume of kink-pair nucleation and migration, thus a high rate sensitivity is typical of bulk BCC metals. Bowout-controlled regime (~ 500 nm $> D > \sim 100$ nm): stress required to bow out a single-arm source overwhelms the lattice friction of screw dislocation, leading to a much smaller rate sensitivity as a result of the large activation volume of single-arm source. Surface/interface-controlled regime ($D < \sim 100$ nm): absence of pre-existing dislocations requires nucleation of dislocations from surface/interface, or non-displacive deformation such as creep, both having small activation volume thus a larger rate sensitivity again.

of residual dislocations in the 1000 nm pillars but few dislocations in the 200 nm pillars. Based on our observations, we proposed that the sample/grain size dependence of m observed in nanostructured BCC metals is mainly a result of the relative magnitudes of dislocation lattice friction and curvature bowout stresses. The latter becomes dominant at small sample (or grain) sizes, entailing a transition of the rate-controlling process (and corresponding activation volume) and hence causing the sample-size-dependent m and the rate-dependent size-strengthening exponent α.

Acknowledgements This research was conducted at Center for Advancing Materials Performance from the Nanoscale (CAMP-Nano) & Hysitron Applied Research Center in China (HARCC), State Key Laboratory for Mechanical Behavior of Materials, Xi'an Jiaotong University, Xi'an 710049, China. Both E.M. and J.L. carried out this work under an adjunct professorship at XJTU.

Disclosure statement No potential conflict of interest was reported by the authors.

Funding This work was supported by the grants from NSFC (51231005, 51321003 and 11132006) and 973 Program of China (2010CB631003, 2012CB619402). We also appreciate the support from the 111 Project of China (B06025). J.L. acknowledges support by NSF DMR-1120901 and DMR-1240933. E.M. was supported at JHU by US-NSF-DMR-0904188.

Supplementary online material A more detailed information on experiments is available at http://dx.doi.org/10.1080/21663831.2014.999953

References

[1] Jia D, Ramesh KT, Ma E. Effects of nanocrystalline and ultrafine grain sizes on constitutive behavior and shear bands in iron. Acta Mater. 2003;51(12):3495–3509.
[2] Cheng GM, Jian WW, Xu WZ, Yuan H, Millett PC, Zhu YT. Grain size effect on deformation mechanisms of Nanocrystalline bcc metals. Mater Res Lett. 2013;1(1):26–31.
[3] Greer JR, Oliver WC, Nix WD. Size dependence of mechanical properties of gold at the micron scale in the absence of strain gradients. Acta Mater. 2005;53(6):1821–1830.
[4] Volkert CA, Lilleodden ET. Size effects in the deformation of sub-micron Au columns. Philos Mag. 2006;86 (33–35):5567–5579.
[5] Kim J-Y, Jang D, Greer JR. Tensile and compressive behavior of tungsten, molybdenum, tantalum and niobium at the nanoscale. Acta Mater. 2010;58(7):2355–2363.
[6] Kim J-Y, Jang D, Greer JR. Insight into the deformation behavior of niobium single crystals under uniaxial compression and tension at the nanoscale. Scripta Mater. 2009;61(3):300–303.
[7] Frick CP, Clark BG, Orso S, Schneider AS, Arzt E. Size effect on strength and strain hardening of small-scale [111] nickel compression pillars. Mater Sci Eng A. 2008;489(1–2):319–329.
[8] Kiener D, Motz C, Rester M, Jenko M, Dehm G. FIB damage of Cu and possible consequences for miniaturized mechanical tests. Mater Sci Eng A. 2007;459 (1–2):262–272.
[9] von Blanckenhagen B, Gumbsch P, Arzt E. Dislocation sources and the flow stress of polycrystalline thin metal films. Philos Mag Lett. 2003;83(1):1–8.
[10] Malow TR, Koch CC, Miraglia PQ, Murty KL. Compressive mechanical behavior of nanocrystalline Fe investigated with an automated ball indentation technique. Mater Sci Eng A. 1998;252(1):36–43.
[11] Wei Q, Cheng S, Ramesh KT, Ma E. Effect of nanocrystalline and ultrafine grain sizes on the strain rate sensitivity and activation volume: fcc versus bcc metals. Mater Sci Eng A. 2004;381(1–2):71–79.
[12] Wei Q, Jiao T, Ramesh KT, Ma E, Kecskes LJ, Magness L, Dowding R, Kazykhanov VU, Valiev RZ. Mechanical behavior and dynamic failure of high-strength ultrafine grained tungsten under uniaxial compression. Acta Mater. 2006;54(1):77–87.
[13] Wei Q, Pan ZL, Wu XL, Schuster BE, Kecskes LJ, Valiev RZ. Microstructure and mechanical properties at different length scales and strain rates of nanocrystalline tantalum produced by high-pressure torsion. Acta Mater. 2011;59(6):2423–2436.
[14] Schneider AS, Clark BG, Frick CP, Gruber PA, Arzt E. Effect of orientation and loading rate on compression behavior of small-scale Mo pillars. Mater Sci Eng A. 2009;508(1–2):241–246.
[15] Weinberger CR, Cai W. Surface-controlled dislocation multiplication in metal micropillars. Proc Natl Acad Sci. 2008;105(38):14304–14307.

[16] Schneider AS, Kaufmann D, Clark BG, Frick CP, Gruber PA, Mönig R, Kraft O, Arzt E. Correlation between critical temperature and strength of small-scale bcc pillars. Phys Rev Lett. 2009;103(10):105501.
[17] Min Han S, Feng G, Young Jung J, Joon Jung H, Groves JR, Nix WD, Cui Y. Critical-temperature/Peierls-stress dependent size effects in body centered cubic nanopillars. Appl Phys Lett. 2013;102(4):041910.
[18] Kim J-Y, Greer JR. Size-dependent mechanical properties of molybdenum nanopillars. Appl Phys Lett. 2008;93(10).
[19] Huang L, Li Q-J, Shan Z-W, Li J, Sun J, Ma E. A new regime for mechanical annealing and strong sample-size strengthening in body centred cubic molybdenum. Nat Commun. 2011;2:547.
[20] Han SM, Bozorg-Grayeli T, Groves JR, Nix WD. Size effects on strength and plasticity of vanadium nanopillars. Scripta Mater. 2010;63(12):1153–1156.
[21] Greer JR, Weinberger CR, Cai W. Comparing the strength of f.c.c. and b.c.c. sub-micrometer pillars: Compression experiments and dislocation dynamics simulations. Mater Sci Eng A. 2008;493(1–2):21–25.
[22] Uchic MD, Dimiduk DM, Florando JN, Nix WD. Sample dimensions influence strength and crystal plasticity. Science. 2004;305(5686):986–989.
[23] Shan ZW, Mishra RK, Syed Asif SA, Warren OL, Minor AM. Mechanical annealing and source-limited deformation in submicrometre-diameter Ni crystals. Nat Mater. 2007;7(2):115–119.
[24] Wang Z-J, Li Q-J, Shan Z-W, Li J, Sun J, Ma E. Sample size effects on the large strain bursts in submicron aluminum pillars. Appl Phys Lett. 2012;100(7):071906.
[25] Suzuki T, Koizumi H, Kirchner HOK. Plastic flow stress of b.c.c. transition metals and the Peierls potential. Acta Metall Mater. 1995;43(6):2177–2187.
[26] Malow TR, Koch CC. Mechanical properties, ductility, and grain size of nanocrystalline iron produced by mechanical attrition. Metall Mater Trans A. 1998;29(9):2285–2295.
[27] Zhang L, Ohmura T, Sekido K, Hara T, Nakajima K, Tsuzaki K. Dislocation character transition and related mechanical response in a body-centered cubic single crystal. Scripta Mater. 2012;67(4):388–391.
[28] Parthasarathy TA, Rao SI, Dimiduk DM, Uchic MD, Trinkle DR. Contribution to size effect of yield strength from the stochastics of dislocation source lengths in finite samples. Scripta Mater. 2007;56(4):313–316.
[29] Jennings AT, Li J, Greer JR. Emergence of strain-rate sensitivity in Cu nanopillars: transition from dislocation multiplication to dislocation nucleation. Acta Mater. 2011;59(14):5627–5637.
[30] Zhu T, Li J, Samanta A, Leach A, Gall K. Temperature and strain-rate dependence of surface dislocation nucleation. Phys Rev Lett. 2008;100(2):025502.
[31] Zhu T, Li J, Samanta A, Kim HG, Suresh S. Interfacial plasticity governs strain rate sensitivity and ductility in nanostructured metals. Proc Natl Acad Sci. 2007;104(9):3031–3036.
[32] Tian L, Li J, Sun J, Ma E, Shan Z-W. Visualizing size-dependent deformation mechanism transition in Sn. Sci Rep. 2013;3:2113.
[33] Sun J, He L, Lo Y-C, Xu T, Bi H, Sun L, Zhang Z, Mao SX, Li J. Liquid-like pseudoelasticity of sub-10-nm crystalline silver particles. Nat Mater. 2014;13(11):1007–1012.